Final Report

Project Title: "High-efficiency Thin-film Fe_2SiS_4 and Fe_2GeS_4-based Solar Cells Prepared from Low-Cost Solution Precursors"

Project Period: 10/01/2013-09/30/2017

Project Budget: $326,139.00

Submission Date: 12/28/17

Recipient: Delaware State University

Address: 1200 N. DuPont Highway, SCS 306,

Dover, DE, 19901

Award Number: DE-EE0006322

Project Team: Daniela R. Radu (Technical lead) and Jadeen Notice (Business lead).

Contacts:

Daniela R. Radu
Associate Professor
Phone: 302-857-6553
Email: dradur@desu.edu

1. Executive Summary:

The project aimed to provide solar energy education to students from underrepresented groups and to develop a novel, nano-scale approach, in utilizing Fe_2SiS_4 and Fe_2GeS_4 materials as precursors to the absorber layer in photovoltaic thin-film devices. The objectives of the project were as follows:

1. Develop and implement one solar-related course at Delaware State University and train two graduate students in solar research.
2. Fabricate and characterize high-efficiency (larger than 7%) Fe_2SiS_4 and Fe_2GeS_4-based solar devices.

The project has been successful in both the educational components, implementing the solar course at DSU as well as in developing multiple routes to prepare the Fe_2GeS_4 with high purity and in large quantities. The project did not meet the efficiency objective, however, a functional solar device was demonstrated.

2. Table of Contents

3. Background:

Solar energy is considered a promising alternative to fossil fuels for its excellent advantages as an abundant, renewable, and clean source of energy. The first silicon solar cell was reported by Russell in 1941,[1] and ever since, silicon solar cells were developed, commercialized and currently account for more than 90 % of solar market. Given the high cost to produce silicon-type solar cells, solar research advanced to the second generation of architectures, comprising thin-film approaches, toward lowering the overall solar cell cost through inexpensive materials and fabrication technologies.[2]

In recent decades, solar energy was considered a promising alternative to fossil fuels for its excellent advantages as an abundant, renewable, and clean source of energy. The first silicon solar cell was reported by Russell in 1941,[1] and ever since silicon solar cells were developed, commercialized and currently account for more than 90 % of solar market. However, given the high cost to produce silicon-type solar cells, solar research advanced to the second generation of constructs, comprising thin-film approaches, toward lowering the overall solar cell cost through inexpensive materials and fabrication technologies.[2] Thin film amorphous silicon, $Cu_2(In,Ga)Se_2$ (CIGS), and CdTe, the three major Gen II solar cells, have been successfully developed and commercialized.[3] Despite their overall success of reaching power conversion efficiencies of up to 22.6 %,[4] CIGS and CdTe solar cells are plagued by the supply limitations and increasing price of rare element indium (In) and gallium (Ga).[5] Besides, both technologies require the use of toxic elements such as selenium (Se) and cadmium (Cd) baring health risks for researchers and manufacturers.[6] Therefore, the demand of alternative, Earth-abundant, non-toxic elements drove the quest for novel absorber materials.

In 1986, pyrite (FeS_2) was viewed as a good alternative to CIGS and CdTe due to its low toxicity, and elements abundance, while offering a large absorption coefficient ($> 10^5$ cm^{-1}) and a band gap suitable for photovoltaic (PV) applications (~ 0.95 eV).[7] Unfortunately, until today pyrite based devices display low power conversion efficiencies of 7 %,[8] which do not match the theoretical efficiency of 20 % and cannot compete with CIGS or CdTe technologies.[9] FeS_2 based solar cell have been impaired by thermal instability,[10] phase-coexistence,[11] and performance problems.[9] Yu et al. pointed to an intrinsic thermal instability of the FeS_2, along with other considerable challenges that must be overcome for obtaining high-quality, single-phase FeS_2 films; the study concluded that for effective solar absorption and henceforth a ligand-field splitting of sufficient magnitude for the Fe^{2+}, the Fe^{2+} ion must be bound by at least six sulfur atoms, requiring the Fe^{2+} cation in an octahedral site. The report predicted that the addition of a third element with an electronegativity favoring strong covalent bonding with sulfur would further stabilize the octahedral site Fe^{2+}. Ge and Si have been demonstrated to fulfill the stabilization requirements, rendering Fe_2SiS_4 and Fe_2GeS_4 compounds which do not readily decompose into S-deficient binary phases.[10] Noteworthy, both materials inherited pyrites superb optoelectronic properties with nearly-ideal bandgaps (Fe_2SiS_4 – calculated: 1.55 eV, measured: 1.54 eV; and Fe_2GeS_4 – calculated: 1.40 eV, measured: 1.36 eV) and similar absorption coefficients ($> 10^5$ cm^{-1}).[10] This suggested the opportunity to work with ultra-thin films, smaller than 1 μm in thickness, along with all the related advantages, including lower materials consumption, homogeneity and impurity control (compared with thicker films), and potential use of flexible substrates.

Moisture sensitivity of Fe_2SiS_4 made its Fe_2GeS_4 (FGS) counterpart, which shows better stability in the air, a better candidate in developing iron chalcogenide PV absorbers.[12]
In addition to the quest for novel thin-film materials, solution processed absorbers have attracted a lot of attention which impacted the new-coming FGS; since Yu's seminal article,[10] predicting FGS potency as a PV absorber, all current reports of FGS materials refer to nanoparticle preparations toward solution processable routes.
Two major synthetic routes for fabricating FGS nanomaterials have been reported: solvothermal,[13,14] and mechanochemical.[15] Prieto's group synthesized FGS nanoparticles through a 24 hours reaction, a fairly long and energy-intensive process. No PV device has been reported, however, the FGS nanoparticles, cast in a thin film, showed a small photocurrent measured by a photo-electrochemical setup.[13] Lim's group synthesized[14] FGS nanosheets trough an alternative solvothermal route, requiring a two-step and 5.5 hour process; the report did not include a PV device. However, the nanosheets exhibited a measured bandgap of 1.38 eV.
In the mechanochemical approach, Park's group synthesized Fe_2GeS_4 nanocrystals in a 12 hours process. The report included Raman scattering experiments revealing a FGS-related peak at 361 cm^{-1}.[15] The post-synthetic annealing of the mechanochemical rendered FGS with a 1.43 eV bandgap.
We are reporting several synthetic methods for preparing Fe_2GeS_4 nanopowders. From the nanomaterials were able to form crystalline Fe_2GeS_4 thin films which enabled fabrication of first Fe_2GeS_4 photovoltaic devices. Our findings reflect the potential of this unexplored material to be employed in thin-film PV.
The successful fabrication of highly crystalline FGS thin films enabled us to construct the first thin-film FGS functional solar device fabricated with a solution based photovoltaic cell. The modest efficiency of the device 0.03 % could be attributed to the overall short-circuit current density (J_{sc}) of 0.19 mA/cm^2, a large open-circuit voltage of 361 mV indicates the potential of FGS as a photovoltaic absorber.

4. Introduction:

In regard to the technical milestones, the project resulted in three facile synthetic routes to Fe_2GeS_4.
A). First method identified the synthetic preparation of nanoprecursor quasi-amorphous powder that, upon annealing in sulfur and argon atmosphere renders pure FGS. The synthesis of precursor powder was highly optimized to produce a stable product. Inks fabricated from the FGS precursor powders were annealed to render highly crystalline FGS thin films.
The successful fabrication of highly crystalline FGS thin films from this powder enabled us to construct the first thin-film FGS functional solar device fabricated with a solution based photovoltaic cell. The modest efficiency of the device 0.03 % could be attributed to the overall short-circuit current density (J_{sc}) of 0.19 mA/cm^2, a large open-circuit voltage of 361 mV indicates the potential of FGS as a photovoltaic absorber.
B). The second approach was the synthesis of FGS nanoparticles via a solvothermal method.
C). The third approach consisted of a solid state molecular precursor approach which involved a novel germanium precursor, Ge glycolate which was synthesized in-house.

A summary of the tasks and milestones that the project followed is presented below (summarized from the Statement of Project Objectives – SOPO).

TASK R-1. Nanoparticles Synthesis

Subtask R-1.1 Nanoparticles Preparation We plan to use nanoparticles to generate the as-made absorber layer Fe_2GeS_4 or Fe_2GeS_4 in p-n junction solar devices.

- ***Subtask R-1.1 Milestone*:**

- Confirm nanoparticles formation (at least Si, Ge and FeS_2) by XRD and demonstrate size distribution control (specifically in the 5-25 nm range); optionally demonstrate formation of Fe_2SiS_4 and Fe_2GeS_4 nanoparticles (XRD).

Subtask R-1.2 Nanoparticles Characterization Successful fabrication of Si, Ge, FeS_2, Fe_2SiS_4 and Fe_2GeS_4 will be determined by the following parameters:

- Composition XRD, TEM-EDS, TGA and ICP-MS will be employed to fully prove the identity and purity of the nanoparticles.
- Size distribution: we aim for a narrow size distribution within each synthetic batch, with particles size <25 nm, more preferred <10 nm. The analysis will be performed by XRD, DLS (dynamic light scattering) and TEM.
- Surface characteristics: The presence and identity of the ligands on the surface will be assessed by FT-IR of pressed nanoparticles pellets and by ligand exchange followed by analyzing supernatants via HPLC and NMR.

- ***Subtask R-1.2 Milestone*:**

- Confirm phase and composition control of Si, Ge and FeS_2 nanoparticle materials and if successful, confirm Fe_2SiS_4 and Fe_2GeS_4 phase, size and stoichiometry.

TASK R-2. Inks and Coatings Preparation. We will prepare inks and use them for coatings on Molybdenum (Mo)-deposited substrates. The coating step will be followed by a thermal processing step. The subtasks include:

Subtask R-2.1 Inks Preparation

We will prepare inks by dispersing the nanoparticles in solvents such as toluene, THF or alpha-terpineol at **100 mg/mL concentration** based on dry nanoparticles weightDynamic Light Scattering (DLS) will assess the aggregation level and sedimentation level will be assessed by visual inspection.

- ***Subtask R-2.1 Milestone*:**

- Demonstrate stable inks for Si, Ge and FeS_2 nanoparticles with shelf life of at least 2 weeks; also for Fe_2SiS_4 and Fe_2GeS_4 if synthesis successful.

Subtask R-2.2 Coatings Preparation

Coatings will be performed by typical coating methods such as spin-coating, rod-coating, or spraying on Mo-coated 1”x1” substrates.

- ***Subtask R-2.2 Milestone*:**

- Demonstrate uniform, continuous (crack-free), single-phase films of ~100 nm deposited on Mo/glass substrate

Subtask R-2.3 Processing

A thermal treatment step will follow the nanoparticles coating

- ***Subtask R-2.3 Milestone*:**

- Deliver a continuous, crack-free, polycrystalline layer of Fe_2SiS_4 and/or Fe_2GeS_4 on a 1"x1" Molybdenum coated substrate and a solar cell structure with the absorber layer made of Fe_2SiS_4 or Fe_2GeS_4 based on CIGS construct that has an efficiency of at least 2%.

Milestone 1 (Task 1&2): Demonstrate a continuous, crack-free, polycrystalline layer of Fe_2SiS_4 and/or Fe_2GeS_4 materials on a 1'x1' Molybdenum coated substrate and a solar cell structure with the absorber layer made of Fe_2SiS_4 or Fe_2GeS_4 based on CIGS construct that has an efficiency of at least 2%.

Go/No-Go Decision Point (24 MONTHS): Deliver a continuous, crack-free, polycrystalline layer of Fe_2SiS_4 and/or Fe_2GeS_4 on a 1"x1" Molybdenum coated substrate **and a solar cell structure with the absorber layer made of Fe_2SiS_4 or Fe_2GeS_4 based on CIGS construct that has an efficiency of at least 2%.**

TASK R-3. Uncover limitations of iron chalcogenides toward performing as theoretically predicted in thin-film PV.

Task R3.1. Identify processing steps that lead to desired stoichiometry in Fe_2SiS_4 or Fe_2GeS_4 annealed films.

Subtask R3.1.1 Evaluate the loss of Ge in Fe_2GeS_4 as model compound and compare with loss of Sn in Cu_2SnS_3 ternary system.

Subtask R3.1.2 Evaluate the loss of Ge in Fe_2GeS_4 obtained from nanoprecursors, mechano-chemical approach (ball milling), and molecular precursors toward establishing route and processing parameters that lead to desired stoichiometry in Fe_2GeS_4.

- ***Subtask R-3.1 Milestone*:** Identify processing parameters that lead to crystalline Fe_2GeS_4 thin film with high purity (>90%).

Task R3.2. Identify minority carrier concentration and carrier lifetime in high purity (>90%) Fe_2GeS_4 thin films.

- ***Subtask R-3.2 Milestone*:** Identify crystalline Fe_2GeS_4 thin film stoichiometry that leads to thin-film acceptable minority carrier concentration and carrier lifetime. (4 months)

Task R3.3. Identify secondary phase and defect distribution in crystalline Fe_2GeS_4 thin films by Raman spectroscopy.

The team will analyze Fe_2GeS_4 thin films by Raman spectroscopy and map the secondary phases and defects.

- ***Subtask R-3.3 Milestone*:** Generate and report on (presentation or peer-reviewed article publication) Fe_2GeS_4 Raman spectra and purity identify secondary phases and defects distribution in crystalline Fe_2GeS_4 thin films obtained in R3.1 and R 3.2.

Educational Milestones

The proposed project will be additive to current efforts by undertaking an initiation step in solar education at DSU. Furthermore, if funded, the project will provide the foundation for starting a solar program at DSU. The project will address two components:

- Development and implementation of a solar-related course in the College of Mathematics, Natural Sciences & Technology at Delaware State University.
- Training of two graduate students in solar research in the context of the proposed research.

The two components will enhance student knowledge and the involvement of members of underrepresented groups in solar science for both the students participating in the PI's research group and the students taught in the proposed class.

The tasks that will be accomplished within the educational scope of the project (E-1, E-2 and E-3 along with subtasks) are presented and detailed as follows.

TASK E-1. *Development of an introductory solar course in the College of Mathematics, Natural Sciences & Technology at Delaware State University*

- ***Task E-1 Milestone:***

- Write student learning outcomes and design appropriate assessments for each outcome.

TASK E-2. **Implementation of the introductory solar course in the College of Mathematics, Natural Sciences & Technology at Delaware State University**

Subtask E-2.1 Course implementation. The course application package will follow the approval process for new courses in the, College of Mathematics, Natural Sciences & Technology at DSU.

- ***Subtask E-2.1 Milestone:***

- Complete course approvals by 06/2014 and complete course implementation by Fall 2014.

Subtask E-2.2 Course evaluation

PI will monitor the course progress from the very first step of implementation. The evaluation will have both a formative and a summative component.

- ***Subtask E-2.2*** Milestone – upon three semesters by December 2015. Generate an evaluation report that captures the results of both formative and summative evaluations and provide an updated syllabus based on results.

TASK E-3. Create a laboratory module to be integrated in the currently offered Solar Materials and Solar cells course and introduce the laboratory-upgraded as mandatory course in the Materials Science and Energy curriculum that is in development.

The College of Mathematics of Natural Sciences and Technology (CMNST) has initiated an "Energy Group". PI Radu is part of the group and has been provided space opportunity and invited to develop a laboratory module for the Solar Materials and Solar cells course she has offered as elective in the Fall 2014.

Final Deliverables:

- **Final Deliverable 1:** Report (presentation or peer-reviewed article publication) findings regarding processing Fe2GeS4 from nanoprecursors, and thin film characteristics: carrier concentration, defect localization, PV device issues, Raman spectroscopy and other limitations of iron chalcogenides toward performing as theoretically predicted in thin-film PV.
- **Final Deliverable 2:** Fully implement an introductory solar course upgraded with laboratory module at DSU as part of the Materials Science curriculum and have at least one article published in a peer-reviewed journal.

5. Project Results and Discussion:

1. Project Overview

- ***Background***

The project aligned with the SunShot goal by offering a cost-effective solution processing approach for Fe_2SiS_4 and Fe_2GeS_4 to build the absorber layer in thin-films PV. The following factors determine the technology cost-effectiveness: **a**. *Materials and processing cost:* materials are composed of earth-abundant elements and the thin-film absorber layer deposition is accomplished by solution-processing; **b**. *Materials properties*: With an estimated direct bandgap of ~1.55 and ~1.4 eV for Fe_2SiS_4 and Fe_2GeS_4 respectively, and an absorption coefficient $>10^5$ cm^{-1}, the materials hold theoretical solar cell efficiency potential comparable with current materials (>20%) and can operate at a 0.1μm required thickness to accomplish similar performance with other thin film materials (such as CIGS)[10]; **c**. *Fabrication and installation costs*: film thickness will significantly contribute to manufacturing and installation costs reduction due to materials light-weight and potential application to flexible substrate.

- ***Objectives***

The proposed project aimed to provide solar energy education to students from underrepresented groups and to develop a novel, nano-scale approach in utilizing Fe_2SiS_4 and Fe_2GeS_4 materials as precursors to the absorber layer in photovoltaic thin-film devices. Objectives are:

1. Develop and implement one solar-related course at Delaware State University and train two graduate students in solar research.

2. Fabricate and characterize high-efficiency (larger than 7%) Fe_2SiS_4 and Fe_2GeS_4-based solar devices.

Technical Research Plan Summary: Sustainable, low-cost materials such as FeS_2 could address environmental and economic concerns raised by amorphous-Si, CdTe and CIGS in thin-film PV. However, to date, FeS_2-based devices show low efficiencies (4%). Alternatively, Fe_2SiS_4 and Fe_2GeS_4 could circumvent these limitations. We will demonstrate a nano-scale approach to Fe_2SiS_4 and Fe_2GeS_4 absorber layers and high-efficiency solar devices (7% or higher). The sustainable, inexpensive iron chalcogenide materials along with solution-processing that could reduce installation costs by enabling use of light-weight, flexible substrates align with SunShot Initiative target of 75% cost reduction in installed PV by 2020.

Education and Workforce Development Plan Summary: The project aimed to develop course instruction in sustainable solar research to minority graduate and undergraduate students. The program success enabled the graduate and undergraduate students involved in research and/or class instruction to acquire both knowledge and a set of skills related to current and emerging industrial solar applications.

- ***Novelty***

Currently there are no reports of Fe_2SiS_4 and Fe_2GeS_4 nanomaterials-based devices. The project novelty consisted of using nano-precursors to build Fe_2SiS_4 and Fe_2GeS_4 absorber layer for thin-film PV via solution processing. Due to <0.1μm required thickness, this new thin-film technology could offer an alternative to other solution-processed materials from abundant elements, such as CZTS which requires 5-8 coating passes to build the absorber layer (as reported by research groups at Solexant, IBM and DuPont).

OUTCOMES OF RESEARCH PLAN (TASKS R1-R3 in SOPO)

A). NOVEL SYNTHESIS OF Fe_2GeS_4 FROM A PRECURSOR AMORPHPUS POWDER (part of this sub-section is from Journal of Materials Science submitted article, currently in revision).

This synthesis route involves fabrication of a nanoprecursor powder that, upon annealing in sulfur and argon atmosphere renders pure ***Fe_2GeS_4***. The synthesis of the precursor powder was highly optimized to produce a stable product. Inks fabricated from the FGS precursor powders were annealed to render highly crystalline FGS thin films.

The successful fabrication of highly crystalline FGS from this powder thin films enabled us to construct the first thin-film FGS functional solar device fabricated with a solution based photovoltaic cell. The modest efficiency of the device 0.03 % could be attributed to the overall short-circuit current density (J_{sc}) of 0.19 mA/cm^2, a large open-circuit voltage of 361 mV indicates the potential of FGS as a photovoltaic absorber. To the best of our knowledge, this is the first functional solar device fabricated with ***Fe_2GeS_4***.

A. 1. EXPERIMENTAL SECTION

Materials. Glycolic acid (99%), diethyl ether (99%), and oleylamine (OLA) (70%) were purchased from Sigma-Aldrich. GeO_2 (99.99%) was purchased from MSE Supplies. Fe(III) 2,4-pentanedionate, sulfur (99.5%) and 1-octadecene (ODE) (90%) were purchased from Alfa Aesar. ACS grade acetone (99.8%), chloroform (99.8%), ethanol

(99.5%), toluene (99.7%) and methanol (99.8%) were purchased from VWR International. Sputtered 0.7 μm molybdenum-coated soda lime grass (Mo-SLG) substrates were obtained from the Institute of Energy Conversion, University of Delaware. Glass substrates were purchased from Fisher Scientific. Indium Tin Oxide (In-SnO2 or ITO) Glass Substrates, 3~5 Ohm/sq, were purchased from MSE Supplies. TiO_2 paste, iodide/tri-iodide electrolyte, and (*cis*-diisothiocyanato-bis (2,2'-bipyridyl-4,4'-dicarboxylato) ruthenium(II) bis (tetrabutylammonium), dye or "*ruthenizer 535-bis TBA"* were purchased from Solaronix. All chemical reagents and solvents were used as received and without further purification.

Synthesis of Diaquabis (glycolato-O,O'') germanium(IV)—$Ge(Gly)_2(H_2O)_2$.

The compound was synthesized through a modified published procedure by Chiang et al.[16] In a typical experiment, germanium dioxide (GeO_2) (0.52 g, 5.0 mmol) was added to a 100 mL pre-prepared aqueous solution of glycolic acid (1.52 g, 20.0 mmol). The reaction mixture was further refluxed for 4 hours. Upon cooling, the final solution was reduced to ~5 mL via rotary evaporation. The $Ge(Gly)_2(H_2O)_2$ powder was precipitated by adding a 1:1 Et_2O: EtOH, and collected by filtration. $Ge(Gly)_2(H_2O)_2$ was store in vacuum.

Synthesis of Fe_2GeS_4 precursor powder with OLA and ODE. In a typical experiment, $Ge(Gly)_2(H_2O)_2$, (0.957 g, 3.73 mmol), 10 mL degassed OLA, and 5 mL ODE were added to a 100 mL two-neck round bottom quartz flask. Separately, Fe(III) 2,4-pentanedionate (2.119 g, 6 mmol) was dissolved in a mixture of 10 mL degassed OLA and 5 mL ODE in a two-neck round bottom glass flask. Sulfur powder (0.384 g, 12 mmol) was dissolved in a mixture of 10 mL degassed OLA and 5 mL ODE in a two-neck round bottom glass flask. Each of the three solutions was stirred at 120 °C for 30 minutes under vacuum to remove moisture. The formed Fe (III) solution was then injected into the Ge(IV) solution at 120 °C and the reaction mixture was held at the same temperature for 10 minutes. Afterwards, the reaction was heated at 250 °C. Meanwhile, the sulfur solution was heated and held at 150 °C. When both solutions reached the target temperatures, the sulfur solution was added drop-wise to the Fe-Ge solution. The final solution was held at 250 °C for 15 minutes. Afterward, the reaction was cooled to room temperature by removing the heating source and the product was purified with a 1:2 $CHCl_3$: ethanol solvent mixture. The resulting solid product was dried under vacuum.

Synthesis of Fe_2GeS_4 precursor powder using OLA. Synthesis of Fe_2GeS_4 precursor powder using OLA followed the same route to the above synthesis but using OLA as solvent instead of a mixture of OLA and ODE.

Preparation of Fe_2GeS_4 powder. The precursor powder obtained with ODE in the synthesis was subjected to a thermal treatment under a sulfur and argon atmosphere in a tube furnace for 2 hours at different temperatures, ranging from 400 °C to 600 °C.

Preparation of Fe_2GeS_4 precursor inks. In a typical experiment, 300 mg of FGS precursor powder was suspended in a mixture of 1.5 mL ethanol and 12 mL toluene, and sonicated for 6 minutes with an ultrasonic probe. The resulting dispersions (inks) were immediately used for films fabrication without further storage.

Fabrication of Fe_2GeS_4 thin films. All films were deposited on either soda-lime glass or Mo-coated soda-lime glass substrates. The substrates were cleaned in an ultrasonic bath using sequentially: methanol, nanopure water, and acetone. Finally, the substrates were dried and subjected to plasma cleaning.

Upon cleaning, each substrate was dip-coated in the FGS precursor ink. Each film has been immersed in the coating ink for 9 times to ensure complete coverage.
Each film was further subjected to thermal treatment under a sulfur and argon atmosphere in a tube furnace for 2 hours at different temperatures, ranging from 400 °C to 600 °C. The sulfur atmosphere was supplied though slow evaporation of sulfur powder, introduced simultaneously with the samples in a crucible placed in the ~ 350 °C zone of the tube furnace.
Solar cell fabrication. The thermally treated films were processed into solar cells using two different approaches. The first approach is a Fe_2GeS_4-catalyzed dye-sensitized solar cell (DSSC) following the approach of Xin et al. who suggested chalcogenide semiconductors to replace the highly expensive platinum as efficient counter electrodes to electro-catalyze solar cell efficiency.[17] Xin et al. and in later reports of other researchers such as Tong et al.[18] showed an efficiency increase in similar constructs using $Cu_2ZnSn(S,Se)_4$ (CZTS), where the improved performance was attributed to an improved short circuit current due to the CZTS-coated counter electrodes.[18] For the present study, TiO_2 films were bar-coated onto fluorine-doped tin-oxide (FTO) substrates and subsequently soft-baked at 300°C for 5 min on a hot plate in order to remove the organic solvent. Afterward, the TiO_2 films were soaked in 0.3 mmol/L ruthenizer 535-bis TBA with methanol, overnight, following a procedure reported by Grätzel's group.[19] The dye-stained TiO_2 film was rinsed with methanol and assembled face-on to the Fe_2GeS_4/Mo thin film in a sandwich-form. Two drops (100 µL) of iodide/ tri-iodide electrolyte were then added into the gap between the two electrodes. The final device had a layered structure shown here: ITO/TiO_2&Dye/Iodine solution/FGS/Mo. In a second approach to make FGS-based solar cells we aimed to decouple the photovoltaic effect of the dye from that of the FGS layer by removing the dye from the solar cell. In order to make this so-called Fe_2GeS_4-solution-based solar cell we repeated all steps from the first approach without adding the dye to the TiO_2 films. This resulted in a final device structure as shown here: ITO/TiO_2/Iodine solution/FGS/Mo.
Characterization. X-ray diffraction (XRD) was performed on a Rigaku MiniFlex600 system equipped with a Cu Kα radiation source **(**λ=1.5405 Å) and operated at 30 mV and 10 mA. Raman spectroscopy analysis was carried out on Horiba Scientific XploRA PLUS equipped with an Ar-laser source (λ = 532 nm). Elemental composition of the dried FGS powder was obtained by X-ray fluorescence (XRF) using a Rigaku Supermini200 model. Room-temperature photoluminescence (PL) spectra were recorded under continuous monochromatic illumination of an argon ion laser (514.5 nm). The PL was collected by two off-axis mirrors, spectrally resolved by a grating monochromator and detected by a Si-CCD array. The current-voltage dependence of the solar cell devices was recorded using a Keithley 2400 source meter under simulated solar light illumination with an intensity of 100 mA/cm^2, generated by a solar simulator (Newport, LCS-100TM).

A. 2. RESULTS AND DISCUSSION

Generation 2 thin film solar cells fabricated through solution methods require an annealing step upon absorber deposition, targeting high-quality, large-grain crystalline absorber layers. Therefore, the crystallinity of precursor materials prior film deposition is not necessarily required. Both solvothermal and mechanochemical synthetic methods

reported to date for producing FGS nanoparticle precursors are time-consuming, cumbersome, and energy-intensive processes,[13-15] therefore, not economically feasible for absorber fabrication. In addition, the absence of a FGS solar device suggests the difficulty to provide robust absorber layers from any nanoparticles reported to date.

Interested in producing crystalline FGS films and PV devices thereon, we have developed a solvothermal method with a 15-minute reaction time, which, after extensive optimization, rendered a precursor powder amenable to produce high purity-FGS upon thermal treatment under sulfur and argon atmosphere.

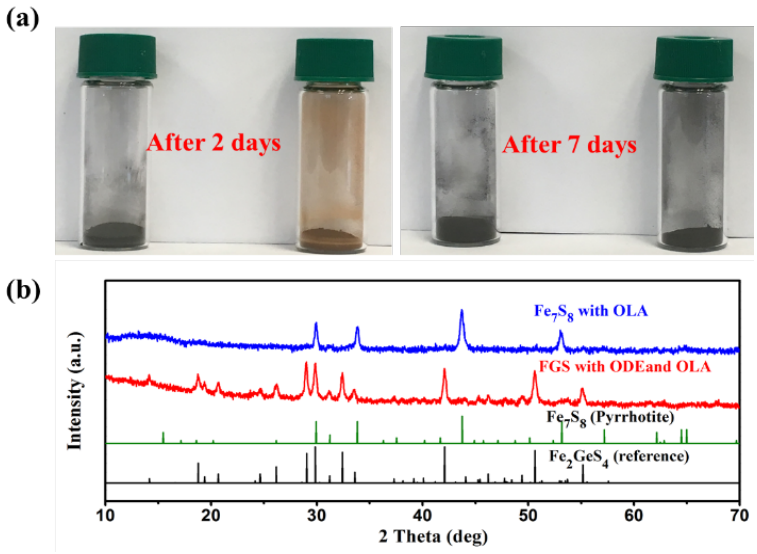

Figure 1. (a) Powder made using OLA as solvent (left) and powder made using a mixture of OLA & ODE (right). (b) XRD patterns of the powders stored in air for OLA (blue) and the OLA & ODE powder stored in air for 7 days (red)

The reaction optimization involved Ge (IV) reagents as well as the solvent system used in the reaction, as follows.

In all FGS precursor powder syntheses, elemental sulfur was used as sulfur source and Fe(III) 2,4-pentanedionate ($Fe(acac)_3$) as Fe(III) source. Two Ge(IV) reagents have been used: The commercially available GeI_4, and the in-house synthesized germanium glycolate, $Ge(Gly)_2(H_2O)_2$. Interestingly, when the synthesis of FGS precursor powder involved GeI_4 as the germanium source, only pyrrhotite was formed, as analyzed by XRD upon powder annealing, whether the OLA or OLA/ODE synthesis was employed, although XRF results indicated Ge presence in the powder. Surprisingly, the use of $Ge(Gly)_2(H_2O)_2$ in the FGS precursor powder synthesis enabled, for the first time, high purity, crystalline powders in the OLA synthesis, using the present precursor powder approach. However, while successful, the method showed poor reproducibility. The reproducibility was not related to the annealing process but to the stability of the FGS precursor powder. As illustrated in Figure 1, if not annealed immediately, the powder showed a fast color change in less than 24 hours. Kauzlarich's group reported that Ge nanoparticles synthesis using alkenes, in particular ODE shows higher stability and resistance to oxidation.[20] Therefore, we introduced ODE in our precursor powder syntheses and the product formed showed tremendous stability improvement, as indicated in Figure 1.

Comparing the XRD patterns of annealed products from both aged powders (Figure 1(b)) it is apparent that the powder obtained from the OLA and ODE mixture remains as a stable Fe_2GeS_4 phase while the powder made from a pure OLA solution decomposes over the timeframe of two days forming pure pyrrhotite ($Fe_{0.789}S$).[21] It should be noted that

XRD measurements obtained from the as-synthesized powders of both procedures (with and without ODE) revealed a quasi-amorphous nature of the powders.
Composition measurements of the synthesized powder from the pure OLA solution revealed the Fe/Ge atomic percent ratio to be 2.3 while the mixed OLA and ODE solution had a Fe/Ge atomic percent ratio of 2.5. In both cases the S/(Fe+Ge) ratio was around 1.2, indicating that the overall composition was close to phase purity with a slight Fe-rich content.
We were further interested in the ability to grow larger crystals through the annealing step and prior depositing the precursor powders in thin films, have performed a study on the precursor (as-synthesized) powders obtained from the mixed OLA and ODE solution approach. The results of this annealing study are illustrated in Figure 2.

By analyzing the XRD patterns it is clear that, independent of the annealing temperature, the predominantly formed phase is FGS. Simulation of XRD patterns (using information about the FGS phase) suggested that a secondary phase is present in all FGS crystalline powder. The best refinement fit for all annealing temperatures was obtained by using the presence of the FGS phase and the $Fe_{0.879}S$ phase. While the mechanism of FGS formation is not the subject of this report, it's important to acknowledge that the olivine FGS does not involve pyrite formation at any step in the process. However, Aydil's group demonstrated that pyrrhotite is detrimental to annealing attempts of pure pyrite, showing that this major impurity is formed at temperatures below 300 °C when annealing pure pyrite films.[21] In FGS's case, the higher the temperature, the less pyrrhotite is formed, suggesting that the presence of Ge does not allow formation of pyrite in this system at any time.
The performed Rietveld analysis also provided a rough comparison of primary crystallite sizes, of around 20 nm at any of the tested temperatures.
When comparing the peak intensity of the two major diffraction peaks of FGS at 28.96° and 29.84° (Figure 2 (b)), it is observed that with increasing annealing temperature, (with the exception of the 600 °C plot) the intensity also increases, indicating that the overall crystallinity of FGS increases and reaches an optimum value at 550 °C and starts to decrease at 600 °C.

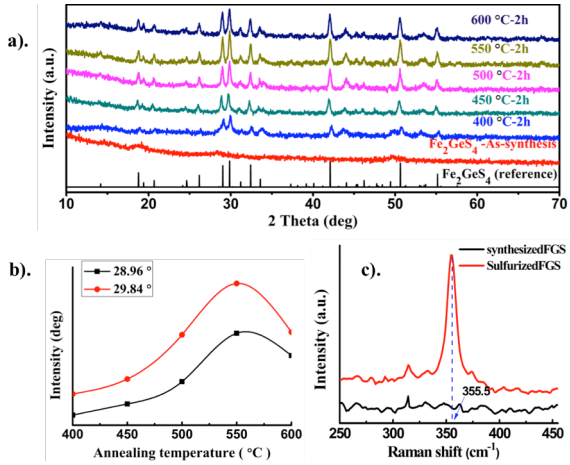

Figure 2. (a) XRD patterns of FGS powder annealed at different temperatures. (b) Intensity comparison of the most intense XRD peaks from the powders annealed at different temperatures. (c) Raman spectra of FGS powder before and after annealing in sulfur/argon at 550 °C 2 h.

The purity of annealed powders was further confirmed by Raman spectroscopy. Figure 2 (c) shows the measured Raman spectra of the FGS precursor powder and the sulfurized FGS powder. The spectrum of sulfurized FGS powder depicts only one significant peak at 355 cm^{-1}, which confirms the peak position of the orthorhombic FGS phase, in agreement with the results reported by Park et al.[15]

Interestingly, Raman peak contributions due to a possible $Fe_{0.879}S$ were not observed, which might suggest that a possible $Fe_{0.879}S$ phase is not surface near.

Toward obtaining films with thickness < 1 μm that could be used in solar cell constructs, FGS thin films were fabricated by dip-coating. The deposited thin films were subsequently annealed in several combinations of temperatures and times, in sulfur/argon atmosphere, similar to the FGS powder. Figure 3 (a) and (b) show XRD patterns from thin films that were annealed at different temperatures and for different times, respectively. Consistent with the annealing study performed on the powders, the thin films also show an optimal annealing temperature of 550 °C. This is indicated by the presence of the two major diffraction peaks of FGS at 28.96° and 29.84° as they are only present for the 550 °C annealing.

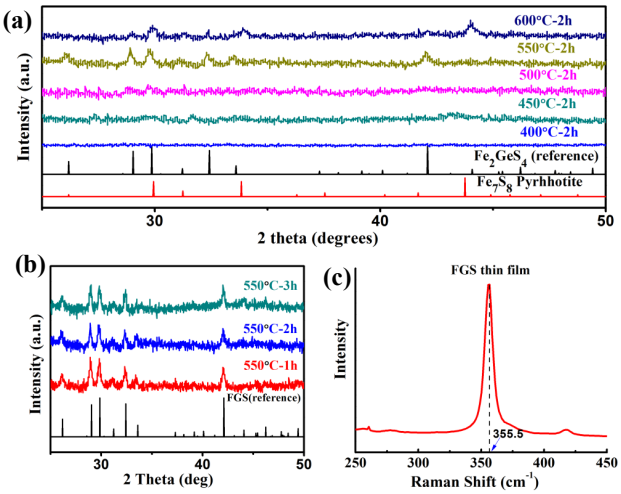

Figure 3. (a) Comparison of XRD patterns of FGS thin film annealed at different temperatures; (b) Comparison of XRD patterns of FGS thin film annealed at 550 °C for different time. (c) Raman of FGS thin film annealed at 550 °C for 2hours

We have further tested if the annealing time impacts crystallinity and stability of the films, at the optimal 550 °C temperature. As depicted in Figure 3 (b), comparing XRD patterns of separate films annealed for one, two, and three hours, respectively, there is a high similarity among the spectra showing no impurity peaks for the samples annealed for 2 hours.

Figure 3 (c) depicts the Raman spectra obtained from the optimally sulfurized Fe_2GeS_4 thin film at 550 °C for 2 hours. A Raman peak at 355.5 cm^{-1} is observed which belongs to the olivine structure of Fe_2GeS_4 phase. These results are in agreement with reported Raman characteristics of FGS.[15]

To validate the bandgap of the FGS materials, photoluminescence (PL) spectroscopy measurements were performed on the two hours annealed film. The overall PL yield was low and in order to remove any effects of the glass substrate on the spectral results, the thin film was lifted off the substrate using a two-component epoxy resin with no luminescence in the spectral region of interest. Figure 4 shows the PL spectra obtained at room temperature after subtracting the background illumination. Despite the low PL yield, a distinct PL peak is observed centered around 1.4 eV, giving a slight indication that the band gap of our FGS thin film is close to the value of 1.4 eV. This is in good agreement with the band gap values of 1.43 eV and 1.38 eV as measured using UV-Vis spectroscopy by Park et al.[15] and Lim et al.[14] using UV-VIS spectroscopy and predicted and measured by Yu et al.[10] As the overall PL yield was too

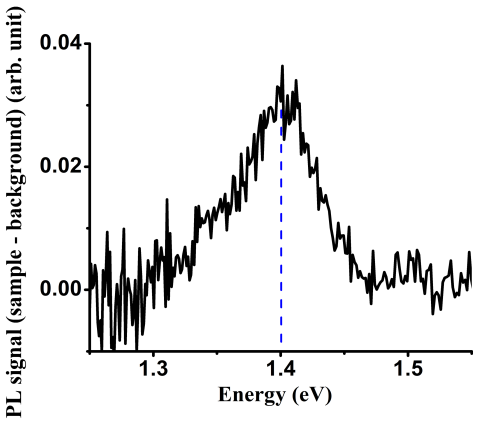

Figure 4. Room temperature PL spectrum of FGS crystalline thin film after subtracting the background.

small, we haven't attempted to measure temperature or intensity dependent photoluminescence spectra; a separate future study will focus on that.

Several recent publications have highlighted the potential of Fe_2GeS_4 to be an excellent candidate for photovoltaic devices,[13-15] yet only one group has been able to measure a FGS-based photocurrent using a photo-electrochemical setup.[13] In the present study, we are showing our results for (i) an FGS-catalyzed dye-sensitized solar cell, and (ii) a solution-based Fe_2GeS_4 solar cell. The first type is based on the approach by Xin et al.[17] who suggested chalcogenide semiconductors to replace platinum as efficient electrocatalyst counter electrodes in DSSC to improve solar cell efficiencies. In the study of Xin et al. and in subsequent studies such as that of Tong et al.[18] it was shown that chalcogenide semiconductors such as Cu_2ZnSnS_4 as a thin film on the counter electrode increases the overall solar cell efficiency by increasing the overall photocurrent. Following this approach we show that FGS is also a suitable candidate for a counter electrode to increase the overall power conversion efficiencies of standard dye-sensitized solar cells by increasing the overall photocurrent [18]. This can be seen in Figure 5 when comparing the light and dark currents of the JV plots in Figure 5 (a) and (b). Figure 5 (b) shows the JV characteristics obtained from a standard dye-sensitized solar cell with the structure: ITO/TiO_2&Dye/Iodine solution/Mo. While the JV curve shows a significant open-circuit voltage (V_{OC}) of 467 mV, the short circuit current density (J_{SC}) of 0.68 mA/cm^2 is fairly low. Introducing a thin film of FGS on the Mo substrate (changing the device structure to ITO/TiO_2&Dye/Iodine solution/FGS/Mo), the V_{OC} increased slightly to 544 mV while the short circuit current increased significantly by a factor of six to 4.15 mA/cm^2, as depicted in Figure 5 (a). This results in an overall power conversion efficiency increase from 0.14 % to 0.71 %, showing the great potential for FGS as a electro-catalyzing material for efficiency improvements in the form of a counter electrode coating for DSSC. The increase in J_{SC} due to the presence of FGS on the counter electrode is speculated to partially be due to the added light absorption in the FGS thin films and partially be due to a higher redox current density of I_3^- to I^- at the counter electrode as compared to the FGS-free counter electrode. This hypothesis is subject of ongoing investigations.

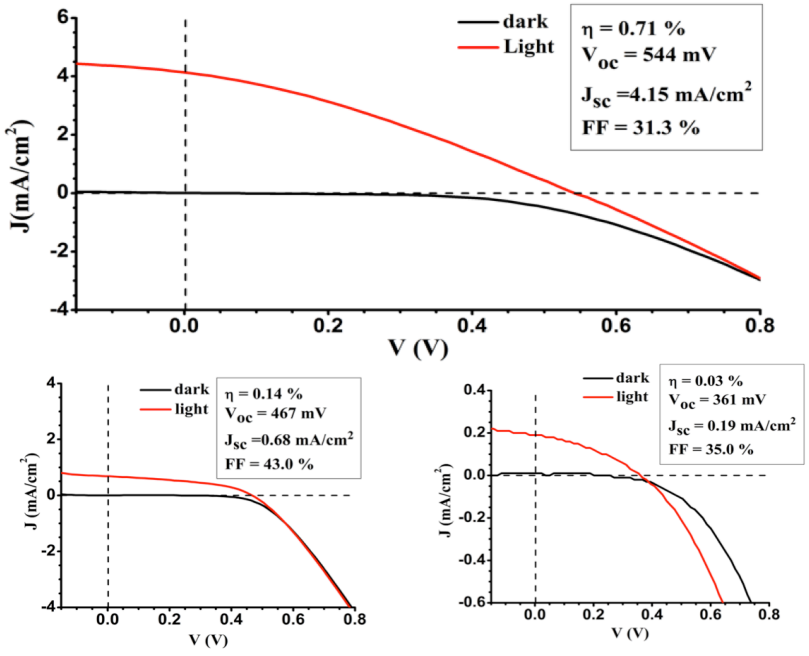

Figure 5. Fe_2GeS_4-catalyzed dye-sensitized solar cell. (a) With FGS thin film; (b) Without FGS thin film; (c) Without dye

In our attempt to decouple the light absorption in the FGS thin films from the light absorption in the dye we have made a FGS solution-based device without the addition of dye to the TiO_2 layer of the following structure: ITO/TiO_2/Iodine solution/FGS/Mo. In this device, the iodine solution is the electrical bridge between the n-type TiO_2 layer and the p-type FGS thin film where the majority of the light absorption is occurring. Figure 5 (c) shows the JV-characteristics in the dark and under illumination for such a solution-based photovoltaic device. Even though the overall short-circuit current density of 0.19 mA/cm^2 under illumination is very low, we measured a large open-circuit voltage of 361 mV resulting in a 0.03 % efficient device. We attribute these very low efficiencies to the very low J_{SC} as the measured open circuit voltage of the device should be high enough to reach efficiencies in the single digit range. Being able to obtain a high V_{OC} from a photoactive material is generally a key property for a photoactive material to be a good candidate for photovoltaic applications. A high V_{OC} means that the used absorbing material is capable of converting photonic energy into an energetic separation of electrons and holes in the conduction and valence bands, respectively. Measuring a V_{OC} of 361 mV for our FGS solution-based devices we can conclude that Fe_2GeS_4 is indeed a good candidate for photovoltaic applications. The low short circuit current measured on our devices indicates that the presented solar cell device structure lacks the ability to extract this converted energy of the energetically separated electrons and holes into physically separating the charge carriers from the absorbing region and driving a current. This ineffectiveness of creating a photocurrent, however, is generally not a good indicator of the potential performance of a photoactive material as such limitations can often be overcome by enhancing and engineering a suitable device architecture around your photoactive material. From this we conclude that the chosen device structure of the solution-based approach might not be the ideal structure for a solar cell based on Fe_2GeS_4. Hence it is our main objective for future research on this material to move away from a solution-based device structure to a solid-state device structure in order to improve photocurrent through an improved charge carrier separation and with it the overall power conversion efficiency. The active area of all solar cell devices made in this work is 2.4 cm^2 and no device optimization has been done yet. The presented results for the open-circuit voltage of this first FGS-based solar cell reaffirms that Fe_2GeS_4 is a promising candidate for a low-cost material for photovoltaic applications and that higher efficiencies are possible with a more suitable solar cell structure. We have performed QE measurements for each of the fabricated devices, with inconclusive results, about the electro-optical properties and potential defects

A. 3. CONCLUSIONS

We presented a solvothermal method with a record reaction time (15 minutes) that produces an amorphous precursor powder to Fe_2GeS_4.
Synthesis optimization suggested that precursor powder stability is highly dependent of Ge(IV) source and the presence of octadecene in the reaction. Annealing of thin films fabricated from the precursor powder under a sulfur/argon atmosphere resulted in crystalline Fe_2GeS_4 thin film. Thermal treatment of 2 hours at 550 °C was found optimal for obtaining high purity Fe_2GeS_4 thin films. Room-temperature photoluminescence measurements of the annealed films showed low PL yield, however, sufficient to identify

a band gap of roughly 1.4 eV for Fe_2GeS_4. When utilized as the counter electrode in dye-sensitized solar cell, Fe_2GeS_4 thin film lead to an enhanced open-circuit voltage and power conversion efficiency. Furthermore, a solution-based solar cell with Fe_2GeS_4 as the absorber layer showed a significant open-circuit voltage of 361 mV highlighting the potentiality of FGS as a photo-active material. A peer reviewed journal article is currently in revisions.

B). SYNTHESIS OF Fe_2GeS_4 NANOPARTICLES VIA A SOLVOTHERMAL METHOD.

B. 1. EXPERIMENTAL SECTION

Materials. The materials utilized in this section largely overlap with the Section A.1; in addition, in B.1. oleic acid (90%), purchased from Aldrich and GeI2 and GeI4 purchased from Gelest have been utilized in the synthesis.
A synthetic approach modified from Lim et. al [14] with inclusion of new reagents such as oleic acid, at a lower temperature (280 °C)and a short reactions time (2 hours) was employed to synthesize **Fe_2GeS_4 nanoparticles. (Liu et al. *Manuscript in preparation*)**

B. 2. RESUTS AND DISCUSSION

The nanoparticles, with average particle size (TEM) of 50 nm showed high purity (XRD and Raman) and have been isolated in gram-size amounts, demonstrating the suitability of the method for scale up.

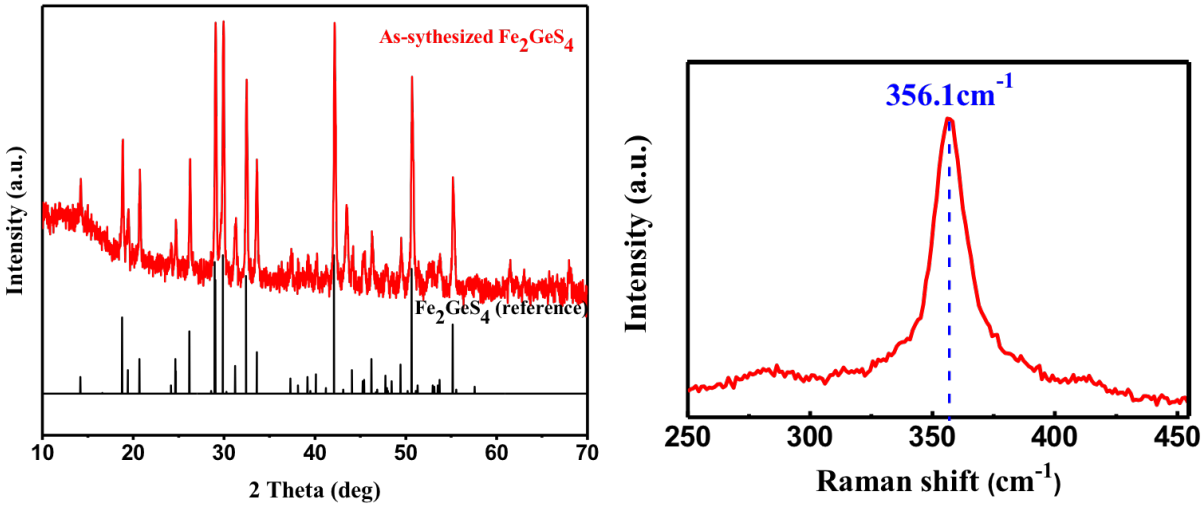

Figure 6. Fe_2GeS_4-Nanoparticles (left) X-Ray diffraction spectrum; (B) Ramsn spectrum of FGS (right)

Figure 6 shows both the XRD and the Raman spectrum of the nanoparticles synthesized in our laboratory.

The material has been further dispersed in suitable solvents to form an ink which was deposited onto Mo-coated soda lime glass, ITO or FTO. Upon annealing the films at 400

°C for 1 hour, UV spectrum has been collected and the bandgap calculation resulted in 1.77 eV, which is slightly above the predicted 1.45 that was reported by Yu et al. (Figure 7) A manuscript is in preparation to be submitted to the Journal of Materials Research.

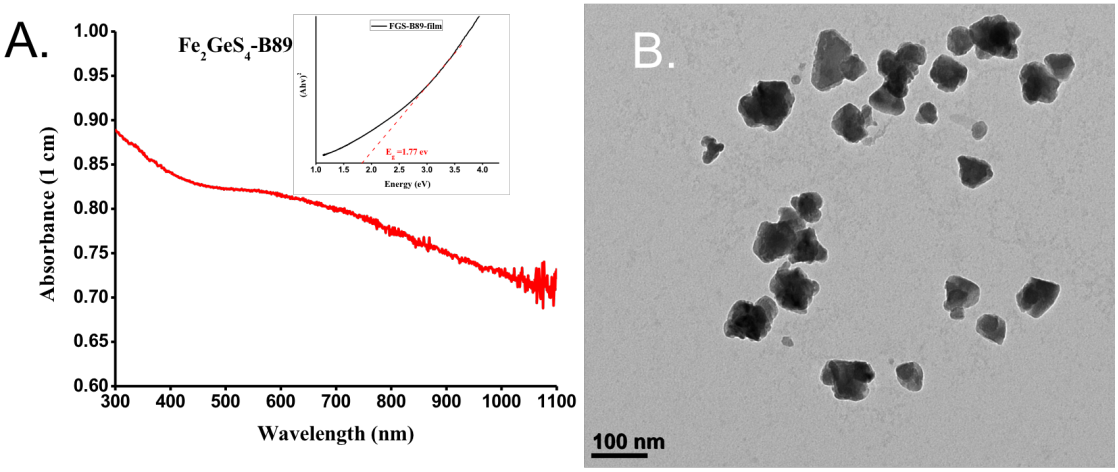

Figure 7. UV –absorbance of FGS Nanoparticles; (A) and TEM of FGS nanoparticles

C. 1.

EXPERIMENTAL SECTION

Materials. Iron (II) acetylacetonate ($Fe(acac)_2$, 99.95%) and ethyl cellulose (EC, 48.0 – 49.5% (w/w) ethoxy basis) was purchased from Sigma-Aldrich. Iron (II) chloride ($FeCl_2$, 99.5%), iron (III) chloride ($FeCl_3$, 98%), and element sulfur (S, 99.5%) were purchased from Alfa Aesar. Diaquabis (oxoacetato-*O, O"*)germanium (IV) (Ge-Gly) was synthesized in-house according to the procedure by Chiang et. al.[16]

Ethanol (200 Proof, 100%) and toluene (>99.5%) were purchased from VWR International.

C. 2. RESULTS AND DISCUSSION

The Fe_2GeS_4 syntheses proposed in the scientific community thus far have either suffered from long reaction times, overly complex reaction procedures, or uncontrollable purity phase changes.[13-15] In order to address these weaknesses we are proposing an optimized solid-state reaction using a hand-grinding technique which significantly reduces the overall reaction time. The utilization of a mechano-chemical reaction to form FGS using a ball-milling approach was investigated by Park et al.[15] showed that ball-milling offers enough mechanical energy to activate the initial chemical reactions between the pulverized elemental precursor materials. The goal of our study is to facilitate and shorten the high purity synthesis of Fe_2GeS_4 nanoparticles using a more efficient short grinding approach in combination with a brief high temperature annealing step which finalizes the FGS solid-state reaction. Our approach uses of molecular compounds as precursors contrary to the element-only synthesis approach pursued by Park et al.[15] In the present research, three series of precursor combination were studied. The first is a so-called "acac-Gly" series that consists of $Fe(acac)_3$, $Ge[(Gly)_2(H_2O)_2]$ and S, the second one is a

so-called "Cl_2-Gly" series that consists of $FeCl_2$, $Ge[(Gly)_2(H_2O)_2]$ and S, and the third one is a so-called "Cl_3-Gly" series that consists of $FeCl_3$, $Ge[(Gly)_2(H_2O)_2]$ and S.

The XRD patterns and the respective Rietveld refinement results of the FGS powder obtained after annealing the product of hand-grinding step of the acac-Gly series at different annealing temperatures are shown in Figure 8(a). It is observed that an annealing at 400 °C for 2 hours only leads to the formation of pyrite (FeS_2, 100 %). Starting at 450 °C, the reaction starts to yield a mixture of Fe_2GeS_4 (39 ± 3 %) together with pyrrhotite (Fe_7S_8, 45 ± 7 %) and pyrite (16 ± 6 %). With increasing annealing temperature, the phase percentage of Fe_2GeS_4 increases further as can be identified by the increase in XRD intensity of the FGS-specific peaks. FGS becomes the majority phase at 500°C, while pyrrhotite decreases in relative abundance. At an annealing temperature of 600 °C, we observe that the minority phase of FeS_2 has completely disappeared, and the formed product is a mixture of the majority phase of Fe_2GeS_4 (72.5 ± 8 %) and a minority phase Fe_7S_8 (27.5 ± 1.9 %). The crystalline size of FGS was estimated to be around 22 nm for the products of almost all annealing temperatures.

The results of the annealing study of the Cl_2-Gly series are summarized in Figure 8(b). At 400 °C three different phases are present, with greigite (Fe_3S_4, 47 ± 5 %), pyrrhotite (35 ± 7 %), and pyrite (18 ± 3%). Pyrite (69.3 ± 4.8 %) replaces greigite as the majority phase at 450 °C and a different phase of pyrrhotite ($Fe_{0.879}S$, 30 ± 3 %) is formed. FGS begins to form around 500 °C as a minority phase (23.8 ± 1.4 %) while pyrrhotite (66.0 ± 0.7 %) replaces pyrite (10.2 ± 0.7 %) as the majority phase. Matching the trends observed in the acac-Gly series, pyrite eventually disappears completely at 550 °C while FGS (42.4 ± 1.1 %) continues to grow relatively. At 600 °C FGS remains the majority phase with 63.9 ± 1.8 % while troilite (FeS, 36.1 ± 0.5 %) remains as minority phase. The estimated crystalline size of FGS for the Cl_2-Gly series with around 34 nm is slightly larger than that of the acac-Gly series.

The annealing study of the third series of hand-grinding to synthesis FGS using the Cl_3-Gly approach, as shown in Figure 8(c) and Table 3, displays a more delayed but also more complete FGS reaction as oppose to previous two series. At 400 °C and 450 °C, pyrite remains the majority phase with 100 % and 73.6 %, respectively, while pyrrhotite (8.9 ± 0.5 %) begins to form at 450 °C as a minority phase. At 500 °C, pyrrhotite (53 ± 4 %) becomes the primary phase as pyrite (47 ± 3 %) decomposes. *Even though FGS (71.9 ± 1.2 %) begins to generate and replace pyrrhotite (28.1 ± 0.9 %) only very late in the process at 550 °C, it eventually becomes the single present phase (100 %) at an annealing temperature of 600 °C*, within the accuracy of the refinement of our measured data. At this point we can only speculate why the Cl_3-Gly approach requires higher annealing temperature to form FGS. *Besides the ability to form single phase FGS powder, this Cl_3-Gly approach further produces crystalline size of around 36 nm.*

The analysis on the three series showcases how the phase stability of the iron sulfide species varies at elevated temperatures. While the temperature to trigger phase change might be different due to different precursor materials, there is one commonly observed trend in all three series: Pyrite as a majority phase always seems to decompose into pyrrhotite species ($Fe_{1-x}S$) with rising temperature. Iron and sulfur can very easily form pyrite at a low temperature which is also the first primary phase we observe at 400 °C.

The onset of pyrrhotite generation that marks the rapid decomposition of pyrite starts at 400 °C and is generally consistent with the report by Zhang et al.[21] The temperature to trigger rapid pyrite decomposition in our approach begins at 450 °C. We hypothesize that this slight difference lies in the presence of germanium species in the form of GeS_2 that

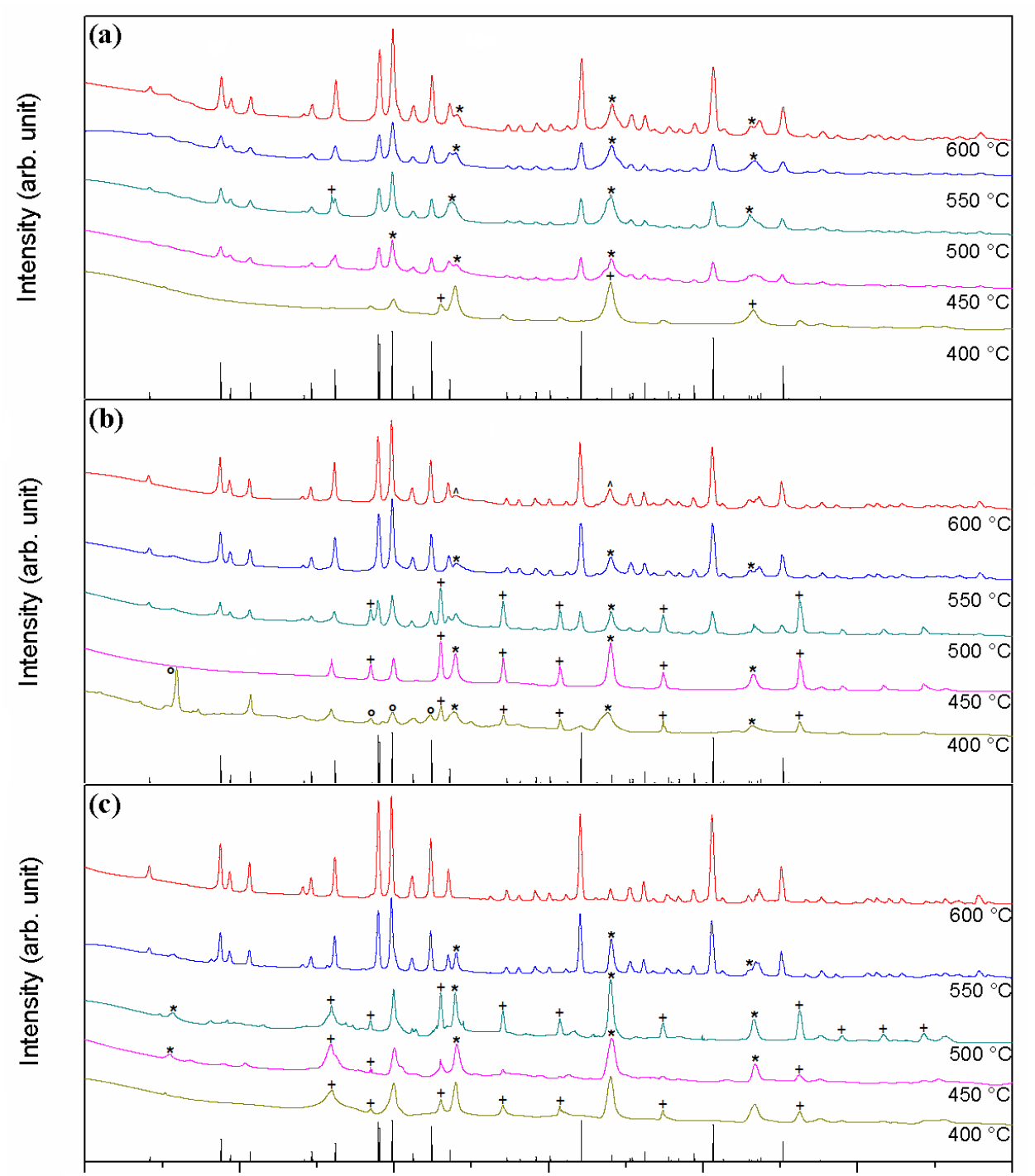

Figure 8. Refined XRD spectra of (a) acac-Gly powder series, (b) Cl_2-Gly, and (c) Cl_3-Gly at elevated annealing temperatures. Each symbol marks a different impurity iron compound phase. The * symbol represents pyrrhotite, the + symbol represents pyrite, the ^ symbol represents troilite, and the ° symbol represents greigite in accordance with the respective phases listed in Tables 1, 2, and 3.

remains amorphous at low temperatures – as noted by Shimada et al. – until being reacted with FGS and ligand groups during the reaction at elevated temperatures as opposed to the phase-pure polycrystalline pyrite FeS_2 films already produced in Zhang et al. [21] The temperatures that initiate the Fe_2GeS_4 formation are also slightly different for the different precursor series. In the acac-Gly series Fe_2GeS_4 starts to form at 450 °C, in the Cl_2-Gly series it forms at 500 °C, and for the Cl_3-Gly series it forms at 550 °C, yet the annealing temperature that prompts Fe_2GeS_4 to become the majority phase is the same across all series at 550 °C. Based on these analyses, we observed that pyrite is consistently first to form at the beginning, but they are quickly converted into pyrrhotite via degradation with the increase of annealing temperature. Further annealing of pyrrhotite leads to the solid-state route synthesis of FGS, and transforms pyrrhotite phases into FGS phase as a majority phase persistently. In the case of Cl_3-Gly series, we observe that a high purity material, a single-phase material of 100%, is obtained following the conversion from the pyrrhotite phase. The consistent conversion of the three phases not only collaborates well with Zhang et. al. with pyrite's tendency to convert into pyrrhotite, it also makes the case that the manipulation of the temperature as a tool to control iron sulfide phase conversions is also realized.

Based on these results, we also see that the usage of iron chloride precursors can lead to drastic improvements to the phase purity of Fe_2GeS_4In our own experiments, FGS, as an iron chalcogenide variant, is also shown to have benefited from the use of halide species, chloride ion in this case, during the annealing process. As seen from the refinement, series with chloride ion presence has higher phase purity at the set temperature of 600 °C. Cl_3-Gly series with the higher presence of chloride ion during annealing outperform the Cl_2-Gly series and acac-Gly series when it came to higher phase purity. Another possibility is described by the hard-soft acid-base (HSAB) theory. The precursors Fe^{2+}, Fe^{3+}, Ge^{4+}, and S are intermediate acid, hard acid, hard acid, and soft base respectively. Fe^{2+} and S will have faster reaction as an intermediate acid and soft base than Ge^{4+} and S as a hard acid to soft base could, meaning the formation of iron sulfide phases will form faster, thus locking out a potential amount of Fe^{2+} to react with Ge^{4+} and S altogether to form Fe_2GeS_4, which means higher chance of generating iron sulfide impurity phases. Fe^{3+} and Cl- as hard acid and hard base delay the reaction for Fe-S due to the complexation between two hard species, which is favorable for fast reaction according to HSAB theory. This delay is beneficial in preventing premature Fe-S reactions that could lead to iron sulfide impurities, leading to better chances of yielding high purity FGS products, which is evident in the case of Cl_3-Gly series.

This study shows that the post-annealing treatment not only promotes crystallinity of the existing phase pure Fe_2GeS_4 phase, as shown previously by Park et al., but it also attributes the conversion of other minority iron sulfide phases into reacting with the amorphous germanium species, thus synthesizing Fe_2GeS_4 nanocrystals. Therefore, the Cl_3-Gly series, with the capability of producing high purity (100%) FGS material at 600 °C, is selected to be the primary approach for making the ink for the subsequent thin film fabrication as discussed below.

As our lab experience has shown, the FGS nanoparticles synthesized with the solid-state procedure are proven difficult and inefficient to be dispersed into typical ink solutions, such as toluene. This is likely due to the large micron sized particle agglomerates that increase the difficulty for particle dispersion which leads to inefficient, long sonication times. Thus, a more efficient approach to ink processing methods has been developed for our material by comparing four different inks.

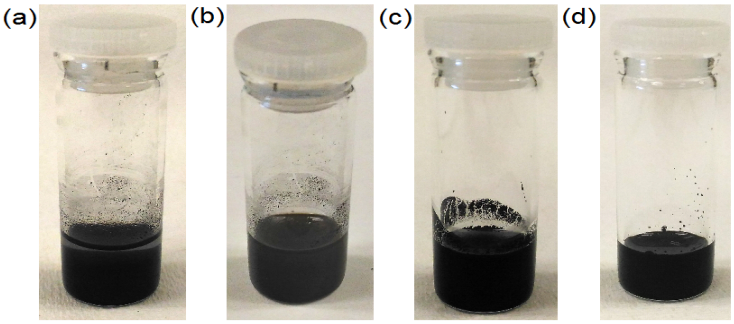

Figure 9. *Photographs of (a) Ink 1, (b) Ink 2, (c) Ink 3, and (d) Ink 4.*

Four ink preparation methods were designed; the components used to formulate the inks are shown in Table 4. Ink 1 follows a typical solar ink processing and is prepared by dispersing Fe_2GeS_4 nanoparticle materials in toluene in a 200 mg/ml concentration via a 20 min sonication [Wang 2014]. Ink 2 is made by dispersing the material in a toluene: α-

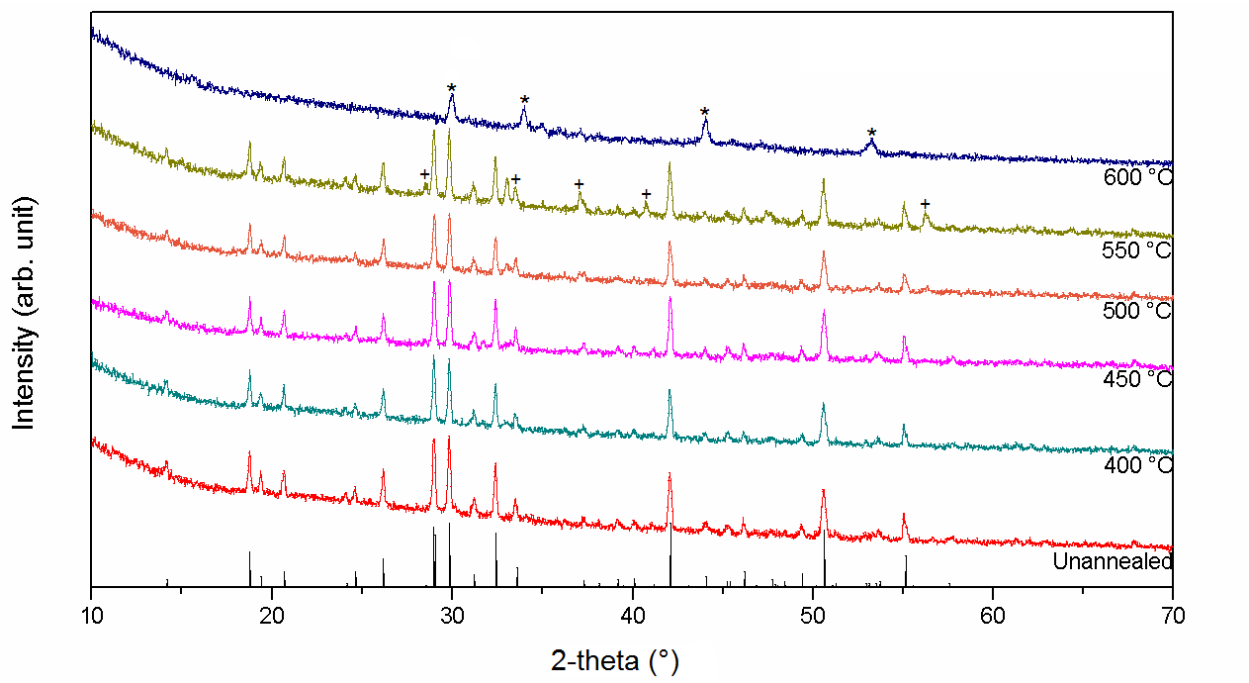

Figure 10. Refined XRD spectra of Film Composition Study of Ink 4 at elevated annealing temperatures. Each symbol marks a different impurity iron compound phase. The * symbol represents pyrrhotite and the + symbol represents pyrite in accordance with the respective phases listed in Table 5.

terpineol (3:1) mixture in a 200 mg/ml concentration via 20 min sonication. Ink 3 is prepared with two solutions. Solution A was prepared with 3:1 ratios of toluene: α-terpineol, and solution B was prepared by dissolving EC (6 wt%) into 4:1 ratios of toluene: ethanol. 1 ml of solution A and 50 µl solution B was mixed and 200 mg of FGS powder was added. The powder is then dispersed with same duration of sonication as Ink 1

following a 20 min sonication, and applied to the substrate via bar-coating. EC was added as an adhesive in the solvent to create better viscosity and promote Fe_2GeS_4 particle suspension. Ink 4 utilizes the same ink solutions in Ink 3, but the mixing is performed using the Flacktek Speedmixer DAC 150.1 FVZ0K. The mixture underwent mixing first at 2500 rotations per minute (RPM) for 5 min, then 3000 RPM for 30 sec of mixing under vacuum.

Ink 1 is shown as inefficient as the required sonication time of 20 min to achieve a thorough dispersion is quite long. The method is also proven unreliable as particles inside the ink precipitate instantaneously, as shown in Figure 9(a). Spin-coating using this ink was not shown to produce even coverage over the substrate and since the material does not fully dissolve, spray-coating is not an option. Bar-coating thus becomes the only viable deposition method and hence is what we have used for all inks in this study.

Ink 2 requires the same long 20 min of sonication duration as Ink 1 to achieve good dispersion, but the utilization of α-terpineol to increase dispersion of the powder material into the solution does provide an increase in dispersion and a good adhesion as discussed below.

Ink 3 is plagued with similarly long sonication times and the lack of dispersions. As shown in Figure 9(c), large aggregates are still observed after sonication and remain as such regardless of further sonication treatment. A bar-coated thin-film suffers from low adhesion, as discussed below.

Ink 4 creates well-mixed and highly viscous ink in less than six minutes of sonication providing high quality and evenly coated thin films on any substrate surface using bar-coating. Grinding the ink mixture with a speedmixer pulverizes the particles which leads to an increase in dispersion of the powder, greatly promoting a very fine ink quality as shown in Figure 9(d). The films deposited using ink 4 shows a greater adhesion between the film and the substrate as compared to thin films processed by the previous inks.

In order to evaluate the inks regarding their suitability to produce thin films for photovoltaic devices, we bar-coated and subsequently annealed films from all four inks and conducted a pull test to determine the adhesion between the thin film and the sample substrate. For this study, all films were annealed inside a tube furnace at 550 °C under atmospheric pressure in the presence of elemental sulfur. The pull test (schematically shown in Figure 12) was performed on a home built setup and it measures the maximum pressure (force per unit area) necessary to vertically lift a metal pin glued to the FGS film from the underlying substrate. The maximum pressure is referred to as the lift-off pressure. Table 4 lists the measured lift-off pressures as obtained by the thin film samples made from the four different inks. The given uncertainty represents the standard deviation of multiple measurements on the same film. The “>” sign in the Tables was always given whenever the film only partially pealed from the substrate and it indicates that the actual lift-off pressure could not be determined fully. As confirmed by Table 4, films created using Ink 1 show overall very poor adhesion ($4.3 \pm 3 \cdot 10^6$ N/m^2). It was further observed that films made using Ink 1 peel off very easily from the substrate, supporting the low adhesion value. Ink 4 by average displays the best adhesion force per unit area ($76 \pm 11 \cdot 10^6$ N/m^2) while Ink 2 leads to an almost equally well adhesion pressure of $54 \pm 36 \cdot 10^6$ N/m^2. Even though Ink 3 is constituted the same as Ink 4, the former performs very poorly due to an

ineffective mixing by sonication. Ink 3 also has a short life-time due to extremely fast precipitation; the powder materials often begin to settle in the solvent in as fast as 5 min. Ink 3 is also noted for the low homogeneity, where clumps of concentrated particles would be seem on the film, creating uneven surfaces. Films deposited using this type of ink lack good adhesion and peel off of the substrate very easily. Ink 4's utilization of a speedmixer allows of full incorporation of ethyl cellulose (EC) into the solution, the adhesion strength has a significant increase as shown in Table 4. In addition, the increase in ink lifetime is also noted as Ink 4 can sustain high homogeneity and viscosity for as long as 20 minutes before it expires as nanoparticles loses dispersion. The expired ink simply needs to be mixed again using a speedmixer with 3000 RPM for 30 sec. As ink 4 has shown the best adhesion results, this ink was selected to be used to study FGS thin films for the use in photovoltaic devices.

In our next step we studied the preferred post-deposition treatment of the deposited thin films in order to observe possible changes in crystallinity of the deposited thin films while removing unwanted residues that were left over from the coating process. For this a series of FGS thin films were bar-coated and subsequently annealed in the presence of sulfur at various temperatures. For this study, all films were made using the Cl_3-Gly series in combination with an annealing step of the powder at 600 °C and using the Ink 4 approach to bar-coat the FGS powder on sample substrates. The deposited thin films were subsequently annealed at a variety of annealing temperatures and structurally analyzed using x-ray diffraction in combination with Raman spectroscopy. The X-ray patterns were compared to calculated pattern using the Rietveld refinement tool of the PDXL software from Rigaku. As part of this series an un-annealed sample was further investigated. All films were annealed in a tube furnace for two hours in a argon atmosphere at ambient pressures and in the presence of elemental sulfur. The Rietveld refinement study of the obtained XRD patterns suggests that post-annealing has detrimental effects to the phase purity, especially for elevated temperatures. As shown in Figure 10, film annealed at 400 °C has Fe_2GeS_4 as majority phase at 88 ± 2% with minority phase of iron pyrite (FeS_2, 12 ± 14%). The films annealed at 450 °C, 500 °C, and 550 °C all retained around 80% Fe_2GeS_4 with a roughly 20 % minority phase of FeS_2. Post-annealing at 600 °C sees a complete decomposition of FGS into pyrrhotite ($Fe_{0.879}S$, 100 ± 8%). Elemental compositional measurements show that germanium still remain in the thin-films past 550 °C, so it is likely that germanium or other germanium sulfide becomes amorphous phases after the post-annealing process. The un-annealed thin film however was shown to retain the single-phase purity (100%) of FGS. Raman spectroscopy supports these findings. Interestingly, the minority, impurity phase generated following the decomposition of Fe_2GeS_4 by post-annealing shows an interesting trend. The first minority phase generated at 550 °C was pyrite, which was completely converted into pyrrhotite at 600 °C along with the rest of the Fe2GeS4 phases. The pyrite-pyrrhotite conversion is consistent with the previous conversion observed during the annealing process to synthesize Fe_2GeS_4. It reaffirms with the above model that pyrite is indeed generally the first phase and degrades into pyrrhotite with the temperature increase, which also confirms with the model provided by Zhang et. al.[21]

Figure 11 depicts the Raman spectra obtained from all annealed and un-annealed thin films. The un-annealed film displays only a high intensity peak at 357 cm^{-1}, indicating the

presence of Fe_2GeS_4 and two small broad peaks at 277 $cm^{-1}$and 315 cm^{-1} indicating that there might be some greigite (Fe_3S_4) present as well. This is not resolved with XRD but as Raman spectroscopy is more surface sensitive than XRD, it is suspected that there might be some small amounts of Fe_3S_4 present at the surface of the thin film. With the increase in annealing temperature, the peak at 357 cm^{-1} gradually decreases in intensity while the two other peak increase. At 550 °C, an additional two peaks at 336 cm^{-1} and 367 cm^{-1} are observed which indicates the generation of iron pyrite (FeS_2) at this temperature as Fe_2GeS_4 degrades. At 600 °C, the peak represents Fe_2GeS_4 is no longer observable, while the peaks at 277 cm^{-1} and 315 cm^{-1} increase in intensity. The results of the Raman study correlate well with the XRD Rietveld refinement study as in both studies the un-annealed thin film appears to have the best quality. Fe_2GeS_4 is also shown to decompose completely at 600 °C in both studies. Based on these results, we can conclude that no or a low temperature thin film post-annealing leads to a better quality FGS film. All annealed and the un-annealed film were further tested in terms of their thin film adhesion. As shown in Table 5, it appears that the films with best adhesion were the un-annealed film ($79 \pm 27 \cdot 10^6$ N/m^2) and the film annealed at 550 °C ($76 \pm 11 \cdot 10^6$ N/m^2). All other films still show good adhesion and do not peel upon touch or handling. As the “greater than” sign (“>”) in the table indicates, it was difficult to put a concrete number on the adhesion as never the whole film underneath the metal pin peeled off but always only very small pieces. The adhesion between some films and the substrate even exceeded that between the glue and the film. In the latter cases, nothing peeled off and as a consequence the adhesion between the thin film and the substrate is greater than the maximum lift-off pressure measured. Overall, we can say that the adhesion on all films prepared using Ink 4 is good with the best results for the films annealed at 550 °C or not annealed at all.

The preparation of FGS thin films comprised a two-step approach by firstly synthesizing FGS powder from a solid state process which subsequently was bar-coated onto a substrate and annealed in a tube furnace. The aforementioned three precursor series are all synthesized in like manner except for the different iron precursors used. In short, the acac-Gly series uses $Fe(acac)_2$ (1.4 g, 4 mmol), Ge-Gly (640 mg, 2.5 mmol) and S (256 mg, 8 mmol). The Cl_2-Gly series uses $FeCl_2$ (507 mg, 4 mmol), Ge-Gly (640 mg, 2.5 mmol) and S (256 mg, 8 mmol). The Cl_3-Gly series uses $FeCl_3$ (648 mg, 4 mmol), Ge-Gly (640 mg, 2.5 mmol) and S (256 mg, 8 mmol). All three series follow the same procedures after this point. The powders were ground by hand with an agate mortar and pestle and mixed under air. The grinding step was performed for 10 minutes, and the product was immediately annealed in an argon atmosphere at elevated temperatures for 2 hours together with 1 g of elemental sulfur and allowed to be naturally cooled down, and then ground to produce the pure Fe_2GeS_4 powder. In order to prepare thin films from the powder we studied several combinations of commonly used solutions for the present work [Wang 2014]. For ink preparation, 200 mg of FGS powder was mixed with 1 ml solvent. For the given study we used the following solvents: a mixture of ethanol, toluene, and α-terpineol.

For

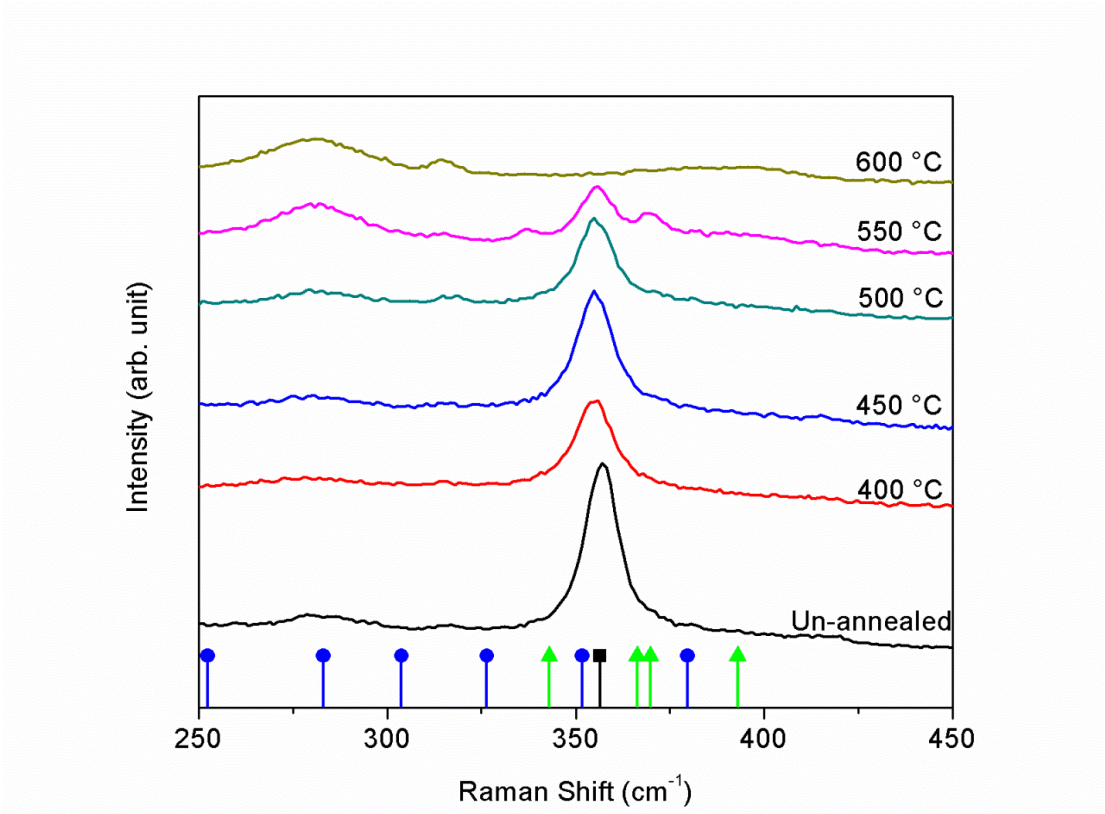

Figure 11. Raman spectroscopy of Film Composition Study of Ink 4 at elevated annealing temperatures. Each symbol and vertical drop-line marks different iron compound phase. The ■ symbol represents reference peaks of Fe2GeS4, the ● symbol represents those of greigite, and the ▲ symbol represents those of pyrite.

further film processing, the FGS ink was applied onto the substrates, glass or molybdenum, via typical bar coating procedure. The substrates were then soft baked at 120 °C on a hotplate for 5 min in air to increase film adhesions. Then, the substrate underwent sulfurization under argon atmosphere at ambient pressures at a variety of elevated temperatures for two hours and in the presence of elemental sulfur. In order to characterize the material properties, all films and powders were analyzed by Rigaku Miniflex 600 X-ray diffraction system CuKα radiation, set at 30 kV and 10 mA. The measured XRD patterns were further matched to simulated XRD pattern using the Rietveld refinement method on the PDXL software provided by Rigaku from which information about the phase composition and crystallite size could be estimated. The Raman spectra were obtained with the XploRa PLUS by Horiba Scientific using the 532 nm laser line. The elemental composition analysis of the annealed thin-film was obtained with X-ray fluorescence (XRF) using a Rigaku Super-mini 200 model. All thin films underwent an adhesion test on a home-built vertical pull setup. The pull test is schematically shown in Figure 12. It measures the maximum pressure (force per unit area glued to the sample) necessary to vertically lift a metal pin glued to the FGS film from the underlying substrate using a force meter that is attached to the hook shown in Figure 12. Commercially available “Gorilla glue ®” was used for the test and it was given at least 12 hours to dry in air before the test was performed. The given numbers are an average over multiple measurements and the given uncertainties in the adhesion study represent the standard deviation of multiple measurements on the same film. PV devices as described

in Section A have been fabricated with this films and results (to be published) were in a similar range of efficiencies.

C. 3. CONCLUSION

The present work proposes a facile solid-state synthesis approach that generates high stability, high phase purity Fe_2GeS_4 nanoparticles. A series of annealing temperature and precursor combination studies were originally conducted to determine the phase purity at annealing temperature stages. However, a reliable phase transformation model was determined following this approach as a consistent trend of pyrite-pyrrhotite-FGS phase conversion is observed between all three species with the increase in annealing temperature. Thus, a case was made that the precise formation of iron sulfide phases is controllable if temperature control is guaranteed.

This study also indicates that the presence of chloride ions is extremely favorable for the crystallization. The consolidation of the two studies provides a reliable pathway for high purity Fe_2GeS_4 nanoparticle material. An optimal ink formulation procedure has been designed specifically for a highly adhesive (> 79 ± 27 $\cdot 10^6$ N/m^2) Fe_2GeS_4 thin film deposition, and post-annealing experiments on the thin-films show the negative effect of post-annealing, highlighting the great quality of the as-deposited thin films.

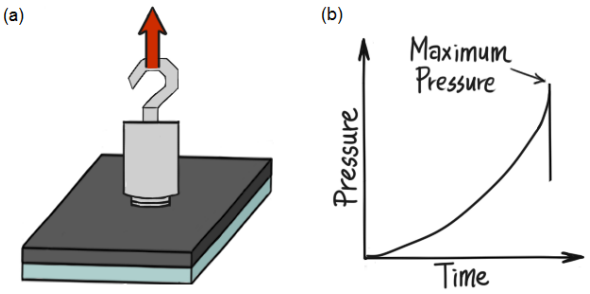

Figure 12. Scheme of the home-built pull tester setup. (a) shows the glued pin to the thin film on the sample substrate. The vertical red arrow indicates the direction of the force applied to the glued pin over time. (b) depicts a sketch of the measured pressure over time. The maximum "lift-off" pressure needed to lift up the substrate from the sample substrate is represented by the highest point in the graph.

This study further underlines the great potential of FGS as a photovoltaic material of the future as we report of high open-circuit voltages (around 400 mV) of the produced photovoltaic devices. Although further optimization is required to increase solar cell device efficiency, the propose method has shown that a solid-state synthesis for Fe_2GeS_4 powder and thin-films has a greater potential for the robust approach, high purity yields, and the immediate solar efficiency response without the need for further treatments on the thin-film.

OUTCOMES OF RESEARCH PLAN (TASKS R1-R3)

TASK E-1. Development of an introductory solar course in the College of Mathematics, Natural Sciences & Technology at Delaware State University

The College of Mathematics, Natural Sciences & Technology (CMNST) at Delaware State University has supported the development of a solar course offered as an elective choice as part of the curriculum for students majoring in Chemistry, Physics and Engineering.

Course Description. The contents of the course brought both a general and an in-depth approach of solar concepts. The course has been offered as a collection of lecture notes

generated based on the materials posted on the PV Education website http://pveducation.org. The materials comprise a comprehensive solar course called PVCDROM that was developed based on NSF funding and is therefore free to use.

TASK E-2. Implementation of the introductory solar course in the College of Mathematics, Natural Sciences & Technology at Delaware State University

Subtask E-2.1 Course implementation.

The course was first taught in the Spring semester 2015 and it is schedule to be offered again with a laboratory module in January 2018.

Subtask E-2.2 Course evaluation

a. Formative Evaluation. The homework, quizzes and midterm exam have been used as tool for the formative evaluation. The instructor defined success as ≥ 75% in percentage students with scores >75%.

b. Summative evaluation. The class presentations and final exam have been used as tool for the summative evaluation along with a course evaluation questionnaire administered (along with the instructor evaluation) at the end of last class.. The evaluation scores reflected high interest (4.3 out of 5) for graduate students and 5.0 out of 5.0 for undergraduate students.

TASK E-3. Training of two graduate students in solar research in the context of the project proposed research

For each material, the assigned student has been trained to:

- Synthesize Fe_2GeS_4 nanoprecursors;
- Generate Fe_2GeS_4 inks from nanoprecursors;
- Deposit coatings on designated substrates;
- Perform thermal treatment of coatings to generate the absorber layer;
- Deposit emitter by solution methods;
- Operate instrumentation at IEC for vacuum deposition of top conductors; Dr. Kevin Dobson, research associate at IEC, will supervise this activity.
- Perform device characterization.

Graduate Student Training Evaluation Plan

- *Research experience*: Both graduate students met expectations to prepare at least one article in a peer-reviewed publication based on results obtained from laboratory work.

Conclusions: The project resulted in three different methods to produce the iron chalcogenide Fe_2GeS_4 in a scalable fashion, with high yield, phase purity and controllable synthetic parameters to avoid formation of the major impurity, pyrrhotite. The work concluded with two peer-reviewed publications and two more manuscripts in preparation (to be submitted in January 2018). Despite the modest efficiency of the reported devices, the V_{oc} values observed in devices produced through all routes,

In regard to educational activities, there are several important accomplishments to highlight: several students have been trained during the project and four visiting scientists have participated, two of them co-authoring the publications resulted from the project.

A course, entitled “Solar Energy and Solar Cells” has been piloted in 2015 as a selective topic course, with dual offering (graduate and undergraduate students) and attracted thirteen undergraduate and four graduate students. A larger investment in renewable energy, in amount of $700,000 from Delmarva Power (State of Delaware’s primary energy distribution company,) occurred in the Spring 2018 towards opening an Renewable Energy and Education Center, equipped with learning kits for students at the university, DSU-affiliated charter high school (DSU Early College High School) and open to public for outreach activities. The laboratory hosting the center will be used for the laboratory module that was prepared as part of the course. Most importantly, a recently awarded NSF grant will support the inauguration of an Energy Engineering degree at DSU (Radu-key personnel).

6. Budget and Schedule: The table below is the summary of the budget periods.

Applicant Name: Delaware State University Award Number: DE-EE0006322.0006 Attachment 3

Budget Information - Non Construction Programs

OMB Approval No. 0348-0044

Section A - Budget Summary

Grant Program Function or Activity (a)	Catalog of Federal Domestic Assistance Number (b)	Estimated Unobligated Funds		New or Revised Budget		
		Federal (c)	Non-Federal (d)	Federal (e)	Non-Federal (f)	Total (g)
1. Budget Period 1				$98,727	$0	$98,727
2. Budget Period 2				$117,121	$0	$117,121
3. Budget Period 3				$110,290	$0	$110,290
4.						
5. Totals				$326,139	$0	$326,139

Section B - Budget Categories

6. Object Class Categories	Grant Program, Function or Activity				Total (5)
	Budget Period 1	Budget Period 2	Budget Period 3		
a. Personnel	$39,889	$30,626	$60,320		$130,835
b. Fringe Benefits	$5,416	$4,593	$5,622		$15,631
c. Travel	$5,000	$2,500	$1,000		$8,500
d. Equipment	$0	$59,000	$0		$59,000
e. Supplies	$9,000	$2,090	$6,170		$17,259
f. Contractual	$0	$0	$0		$0
g. Construction	$0	$0	$0		$0
h. Other	$10,050	$0	$2,430		$12,480
i. Total Direct Charges (sum of 6a-6h)	$69,354	$98,809	$75,541		$243,705
j. Indirect Charges	$29,373	$18,312	$34,749		$82,434
k. Totals (sum of 6i-6j)	$98,727	$117,121	$110,290		$326,139
7. Program Income	$0	$0	$0		$0

SF-424A (Rev. 4-92)
Previous Edition Usable Prescribed by OMB Circular A-102
Authorized for Local Reproduction

Budget discussion. The project did not involve cost share from the University or other sources. The total awarded funds were **$326,139.00** all federal Share. The total expenditures, as reflected in the final financial report, is: **$319,772.03.**

Provided the delay in drawing funds after budget Period 1&2, the project was placed in

No-cost extension in Budget period 2, which was extended to 03/31/2017; the budget periods have been modified as follows:

Budget Period 1: 09/30/2013 to 09/30/2014
Budget Period 2: 10/01/2014 to 03/31/2016
Budget Period 3: 04/01/2016 to 03/31/2017

Upon the no cost extension period passed, DSU requested approval for continuation and approval was granted along with a modification of the Budget Period 3 as follows:

Budget Period 1: 09/30/2013 to 09/30/2014
Budget Period 2: 10/01/2014 to 03/31/2016
Budget Period 3: 04/01/2016 to 09/30/2017

7.Path Forward: In future research, we will focus on a solid state solar cell device structure in order to improve J_{SC} through an improved charge carrier separation and with it the overall power conversion efficiency.

In addition, in the process of fabricating the *olivines Fe_2SiS_4 and Fe_2GeS_4*, we observed *formation of ultra-thin films of pyrite that incorporated only 1.5%Ge (by EDX) and showed p-type conduction*.

Surprisingly, we noticed that thermal treatment, when performed under sulfur atmosphere, prevented degradation and rendered films that are stable in ambient conditions. The observation has prompted us to consider doping as a solution to both driving the pyrite conduction to p-type and to achieve chemical stabilization of pyrite.

Doping in naturally-occurring pyrite. Nature demonstrates (data from geological and geochemistry reports) that naturally occurring pyrite, the "fool's gold" is either n- or p-type, as a function of impurities in the compound. For instance, pyrites from sedimentary and epithermal deposits are usually p-type if cupriferous sulfides are not present. Samples from hypothermal deposits are usually n-type if there are no antimony minerals in the ore.[22] More specifically, naturally-occurring pyrites enriched in cobalt are an n-type

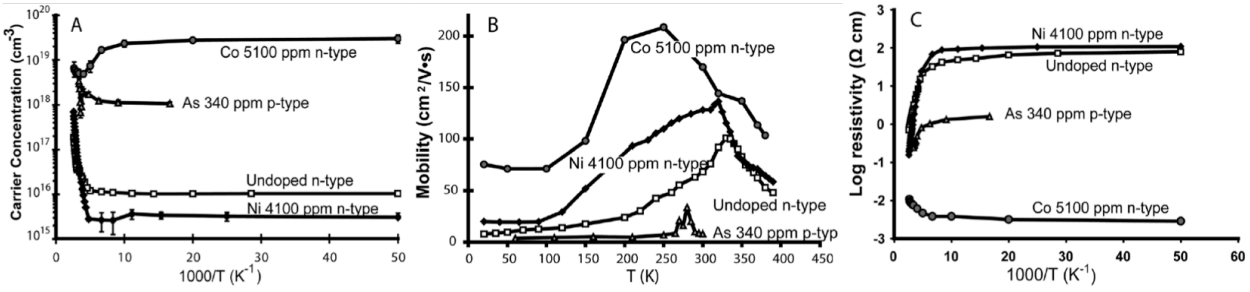

Figure 13. Electronic properties of Ni, Co and As-doped Pyrite (From ref. [24])

semiconductors with low resistivity and high carrier mobility, while arsenic (As) containing pyrites are p-type and has higher resistivity.[23] The increase in occurrence of p-type conductivity with increasing **As** concentration supports the reported hypothesis that **As** substitutes for S in the pyrite structure introducing empty orbitals into the band gap near

the valence band. The synchrotron XRD data indicate an expanded lattice for arsenic-doped pyrite which is consistent with As substitution for S.[24]
Geochemists' research in this arena, motivated primarily by understanding how compositional impurities influence the oxidation of pyrite in nature[24], have been purposely doping and studying electronic properties of Ni, Co and As-doped (as individual, not collective dopants) obtained by chemical vapor deposition (CVD).

As indicated in Figure 13, Co, As and Ni-doped materials show that doping could determine conduction to p- or n-type. At the dopant concentrations pursued in the report (~molar 1% for Co and as low as ~0.05% for As), doping helps to decrease resistivity in intrinsic in respect to the undoped pyrite while increasing carrier concentration. Notably, several other reports also indicate that growth of large crystals via either flux, sulfidation or solid state synthesis, lead to n-type bulk pyrite.[21]
These finding suggest that doping pyrite nanocrystals is chemically permitted at various concentrations and suggest an excellent future approach to finally converting pyrite, also known as "fool's gold", into a useful photovoltaic material.

8. Publications Resulting from This Work:

1. Chen, C.-C.; Stone, K. H.; Lai, C.-Y.; Dobson, K. D.; Radu, D. Sulvanite (Cu3VS4) nanocrystals for printable thin film photovoltaics. *Materials Letters* **2018**, *211*, 179-182.
2. Liu, Mimi, Berg, Dominik; Hwang, Po-Yu; Lai, Cheng-Yu; Babbe, Finn; ; Dobson, Kevin, Radu, Daniela, The Promise of Solution Processed Fe_2GeS_4 Thin Films in Iron Chalcogenide Photovoltaics, Journal of Materials Science, *in revision*

9. References:

(1) Ohl, R. Light-Sensitive Electric Device Including Silicon. US Patent.
(2) Chopra, K. L.; Das, S. R.: Why Thin Film Solar Cells? In *Thin Film Solar Cells*; Chopra, K. L., Das, S. R., Eds.; Springer US: Boston, MA, 1983; pp 1-18.
(3) Ullal, H. S.; von Roedern, B. In *Tilte*, United States, 2007-09-01, 2007: Research Org.: National Renewable Energy Laboratory (NREL), Golden, CO., Sponsor Org.: USDOE.
(4) Green, M. A.; Emery, K.; Hishikawa, Y.; Warta, W.; Dunlop, E. D.; Levi, D. H.; Ho-Baillie, A. W. Y. Solar cell efficiency tables (version 49). *Progress in Photovoltaics: Research and Applications* **2017**, *25*, 3-13.
(5) Fthenakis, V. Sustainability of photovoltaics: The case for thin-film solar cells. *Renewable and Sustainable Energy Reviews* **2009**, *13*, 2746-2750.
(6) Nguyen, K. C.; Willmore, W. G.; Tayabali, A. F. Cadmium telluride quantum dots cause oxidative stress leading to extrinsic and intrinsic apoptosis in hepatocellular carcinoma HepG2 cells. *Toxicology* **2013**, *306*, 114-123.
(7) Ennaoui, A.; Fiechter, S.; Jaegermann, W.; Tributsch, H. Photoelectrochemistry of Highly Quantum Efficient Single-Crystalline n-FeS2 (Pyrite). *Journal of The Electrochemical Society* **1986**, *133*, 97-106.
(8) Kilic, B.; Turkdogan, S. Fabrication of dye-sensitized solar cells using graphene sandwiched 3D-ZnO nanostructures based photoanode and Pt-free pyrite counter electrode. *Materials Letters* **2017**, *193*, 195-198.

(9) Ennaoui, A.; Fiechter, S.; Pettenkofer, C.; Alonso-Vante, N.; Büker, K.; Bronold, M.; Höpfner, C.; Tributsch, H. Iron disulfide for solar energy conversion. *Solar Energy Materials and Solar Cells* **1993**, *29*, 289-370.

(10) Yu, L.; Lany, S.; Kykyneshi, R.; Jieratum, V.; Ravichandran, R.; Pelatt, B.; Altschul, E.; Platt, H. A. S.; Wager, J. F.; Keszler, D. A.; Zunger, A. Iron Chalcogenide Photovoltaic Absorbers. *Advanced Energy Materials* **2011**, *1*, 748-753.

(11) Wang, H.; Salveson, I. A review on the mineral chemistry of the non-stoichiometric iron sulphide, Fe1− x S ($0 \leq x \leq 0.125$): polymorphs, phase relations and transitions, electronic and magnetic structures. *Phase Transitions* **2005**, *78*, 547-567.

(12) Jieratum, V. Ph.D. Thesis. *Oregon State University* **2012**.

(13) Fredrick, S. J.; Prieto, A. L. Solution Synthesis and Reactivity of Colloidal Fe2GeS4: A Potential Candidate for Earth Abundant, Nanostructured Photovoltaics. *Journal of the American Chemical Society* **2013**, *135*, 18256-18259.

(14) Lim, D.-H.; Ramasamy, P.; Lee, J.-S. Solution synthesis of single-crystalline Fe2GeS4 nanosheets. *Materials Letters* **2016**, *183*, 65-68.

(15) Park, B.-I.; Yu, S.; Hwang, Y.; Cho, S.-H.; Lee, J.-S.; Park, C.; Lee, D.-K.; Lee, S. Y. Highly crystalline Fe2GeS4 nanocrystals: green synthesis and their structural and optical characterization. *Journal of Materials Chemistry A* **2015**, *3*, 2265-2270.

(16) Chiang, H. C.; Wang, M. H.; Ueng, C. H. Synthesis and structure of diaquabis(glycolato-O,O'')germanium(IV). *Acta Crystallographica Section C* **1993**, *49*, 244-246.

(17) Xin, X.; He, M.; Han, W.; Jung, J.; Lin, Z. Low-cost copper zinc tin sulfide counter electrodes for high-efficiency dye-sensitized solar cells. *Angew Chem Int Ed Engl* **2011**, *50*, 11739-11742.

(18) Tong, Z.; Su, Z.; Liu, F.; Jiang, L.; Lai, Y.; Li, J.; Liu, Y. In situ prepared Cu2ZnSnS4 ultrathin film counter electrode in dye-sensitized solar cells. *Materials Letters* **2014**, *121*, 241-243.

(19) Kalyanasundaram, K.; Grätzel, M. Efficient dye-sensitized solar cells for direct conversion of sunlight to electricity. *Material Matters* **2009**, *4*, 88-90.

(20) Nolan, B. M.; Chan, E. K.; Zhang, X.; Muthuswamy, E.; van Benthem, K.; Kauzlarich, S. M. Sacrificial Silver Nanoparticles: Reducing GeI2 To Form Hollow Germanium Nanoparticles by Electroless Deposition. *ACS Nano* **2016**, *10*, 5391-5397.

(21) Zhang, X.; Scott, T.; Socha, T.; Nielsen, D.; Manno, M.; Johnson, M.; Yan, Y.; Losovyj, Y.; Dowben, P.; Aydil, E. S.; Leighton, C. Phase Stability and Stoichiometry in Thin Film Iron Pyrite: Impact on Electronic Transport Properties. *ACS Applied Materials & Interfaces* **2015**, *7*, 14130-14139.

(22) Donald F. Pridmore, R. T. S. The electrical resistivity of galena, pyrite, and chalcopyrite. *American Mineralogist* **1976** *61*, 248-259.

(23) Savage, K. S.; Stefan, D.; Lehner, S. W. Impurities and heterogeneity in pyrite: Influences on electrical properties and oxidation products. *Applied Geochemistry* **2008**, *23*, 103-120.

(24) Lehner, S. W.; Savage, K. S.; Ayers, J. C. Vapor growth and characterization of pyrite (FeS2) doped with Co, Ni, and As: Variations in semiconducting properties. *J. Cryst. Growth* **2006**, *286*, 306-317.